

# Revisiting the global surface energy budgets with maximum-entropy-production model of surface heat fluxes

Shih-Yu Huang<sup>1</sup>  · Yi Deng<sup>2</sup> · Jingfeng Wang<sup>1</sup>

Received: 19 August 2016 / Accepted: 7 October 2016 / Published online: 18 October 2016  
© Springer-Verlag Berlin Heidelberg 2016

**Abstract** The maximum-entropy-production (MEP) model of surface heat fluxes, based on contemporary non-equilibrium thermodynamics, information theory, and atmospheric turbulence theory, is used to re-estimate the global surface heat fluxes. The MEP model predicted surface fluxes automatically balance the surface energy budgets at all time and space scales without the explicit use of near-surface temperature and moisture gradient, wind speed and surface roughness data. The new MEP-based global annual mean fluxes over the land surface, using input data of surface radiation, temperature data from National Aeronautics and Space Administration–Clouds and the Earth’s Radiant Energy System (NASA CERES) supplemented by surface specific humidity data from the Modern-Era Retrospective Analysis for Research and Applications (MERRA), agree closely with previous estimates. The new estimate of ocean evaporation, not using the MERRA reanalysis data as model inputs, is lower than previous estimates, while the new estimate of ocean sensible heat flux is higher than previously reported. The MEP model also produces the first global map of ocean surface heat flux that is not available from existing global reanalysis products.

**Keywords** Maximum entropy production model · Global surface energy budget · Surface heat fluxes · Ocean heat flux estimation

## 1 Introduction

One major challenge in the study of global climate change is monitoring and modeling surface water and energy budgets. Two recent studies (e.g., Trenberth et al. 2009; Stephens et al. 2012) summarized our current knowledge about global annual mean water and energy budgets. These studies conclude that the existing estimates of the surface (radiative and turbulent) fluxes have substantial uncertainties and do not close the surface energy budget. Uncertainties of the surface turbulent fluxes are in general twice as large as those of surface radiative fluxes. In addition, there are “no estimates of the sensible heat fluxes over the polar regions of sea ice” and no estimates of surface water heat fluxes over oceans. The estimates of global surface energy fluxes at sub-annual time scales are expected to have even higher uncertainties.

The difficulties in obtaining accurate estimates of surface turbulent heat fluxes are arguably resulting from the drawbacks of the fluxes models. The turbulent fluxes over the Earth–atmosphere interface are commonly modeled using the bulk transfer method (e.g., Arya 1988). Further improvement of the bulk fluxes faces theoretical and technical obstacles. Bulk fluxes in general do not conserve energy (and mass)—the primary cause of unbalanced surface energy budget. Large measurement errors of the bulk gradients between surface and near-surface temperature and humidity directly lead to the uncertainties of the bulk fluxes. Empirical transfer coefficients in the bulk transfer formula add more uncertainties to the bulk fluxes. Specifically, parameterization of transfer coefficients in terms of wind speed and surface roughness length(s) (SRL) may cause substantial errors in the bulk fluxes. Renfrew et al. (2002) showed that the parameterization of SRL used to compute bulk transfer coefficient in the National Centers for Environmental

---

✉ Shih-Yu Huang  
shuang83@gatech.edu

<sup>1</sup> School of Civil and Environmental Engineering,  
Georgia Institute of Technology, 790 Atlantic Drive,  
Atlanta, GA 30332-0355, USA

<sup>2</sup> School of Earth and Atmospheric Sciences,  
Georgia Institute of Technology, Atlanta, GA, USA

Prediction (NCEP) bulk algorithm leads to overestimations of turbulent heat fluxes (latent and sensible) under moderate to high wind speed conditions. The effects of wind speed biases on bulk fluxes have been shown to be most pronounced in winter months (Moore and Renfrew 2002). Wind speed also affects the bulk fluxes through the parameterization of SRL. Earlier studies (Zeng et al. 1998; Renfrew et al. 2002) suggested that commonly used formulae of SRL have difficulties in producing consistent estimates of surface momentum and heat fluxes, especially heat fluxes, under weak wind as well as moderate to high wind conditions. Besides, measuring of wind speed and surface roughness over large regions are difficult. Remote sensing retrievals of surface wind speed based on, for example, the empirical relationship between wind speed and ocean surface roughness are known to be subject to substantial biases and uncertainties (Katzberg et al. 2001; Komjathy et al. 2004; Katzberg and Dunion 2009; Clarizia et al. 2012). Lack of energy conservation is a fundamental drawback of the bulk fluxes with no obvious solution. The measurement error of a bulk gradient computed from the difference of two close numbers is also difficult to reduce given existing technology. Even if all bulk gradient variables are free of measurement errors, the bulk fluxes have inherent modeling errors since the bulk transfer models are based on the first-order closure of the Reynolds decomposition of turbulent flows subject to substantial and unknown modeling errors. Closure problem in turbulence models remains “one of the unsolved problems in classical physics” (Stull 1988). As a result, the estimation errors of bulk fluxes are often unbounded without the constraint of surface energy balance.

A new innovative approach, the maximum entropy production (MEP) model (Wang and Bras 2009, 2011; Wang et al. 2014), was recently developed to overcome the drawbacks of the existing approaches. The foundation of the MEP model is the contemporary non-equilibrium thermodynamics built on the Bayesian probability theory, information theory and well established atmospheric boundary layer turbulence theory. In the MEP model, the surface turbulent and/or conductive energy fluxes effectively result from the partitioning of radiation fluxes automatically balancing the energy budget. The modeling errors of the MEP fluxes are bounded by the measurement errors of surface radiation fluxes. As the first humidity (and temperature)-gradient independent, physically-based model of evaporation, the MEP model does not make explicit uses of near-surface water vapor deficit (and temperature gradients) data to avoid the substantial measurement errors of the bulk gradient variables. The MEP model also uses fewer model parameters (than existing models) that are independent of wind speed and SRLs. With its theoretical and technical advantages, the MEP model provides a promising new

method to meet the challenge of monitoring and modeling global surface energy fluxes.

In this study, the global climatology of the surface heat fluxes together with the corresponding uncertainties is re-estimated using the MEP model utilizing the input data of radiation and temperature from the National Aeronautics and Space Administration (NASA) Clouds and the Earth’s Radiant Energy System (CERES) products supplemented by the (land) surface specific humidity data from the NASA Modern-Era Retrospective analysis for Research and Applications (MERRA) products. The MEP estimated climatology of surface heat fluxes will be compared with previous estimates. Since surface heat fluxes data over the polar regions do not exist, the analyses of the MEP surface heat fluxes exclude the contributions from the polar regions for the purpose of consistency.

## 2 Method and data

### 2.1 Surface energy balance equations

The energy balance equations over the Earth surface depend on the transparency of the surface material to sunlight. Over the land masses (Fig. 1a) where surface media are non-transparent to sunlight, the conservation of energy at the land–atmosphere interface is expressed as,

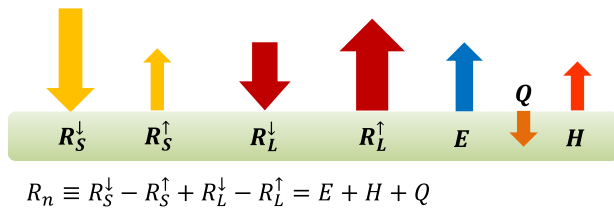
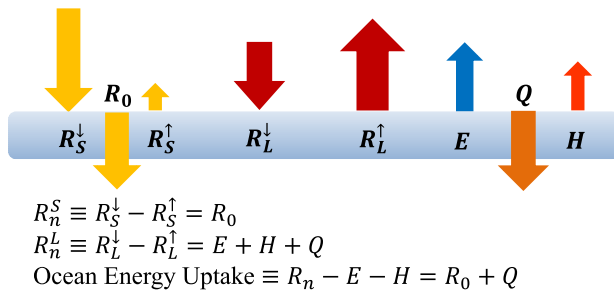
$$E + H + Q = R_n \equiv R_S^\downarrow - R_S^\uparrow + R_L^\downarrow - R_L^\uparrow, \quad (1)$$

where  $R_n$ ,  $R_S^\downarrow$ ,  $R_S^\uparrow$ ,  $R_L^\downarrow$ , and  $R_L^\uparrow$  are net radiation, incoming solar, reflected solar, downward atmospheric long-wave and surface emitted long-wave radiation, respectively. The radiative fluxes towards the surface are defined as positive. Latent  $E$ , sensible  $H$  and ground heat  $Q$  fluxes entering the atmosphere and/or soil layer are defined as positive.

Over water, snow, and ice surfaces (Fig. 1b) where the surface media are transparent to sunlight, the conservation of energy is expressed as (e.g., Badgley 1966; Saunders 1967; Weller 1968; Fairall et al. 1996; Wang et al. 2014),

$$\begin{aligned} E + H + Q &= R_n^L \equiv R_L^\downarrow - R_L^\uparrow, \\ R_0 &= R_n^S \equiv R_S^\downarrow - R_S^\uparrow \end{aligned} \quad (2)$$

where  $R_0$  is the (net) solar radiation entering the (water–snow–ice) media equal to  $R_n^S$ ,  $R_n^L$  the net long-wave radiation,  $Q$  the surface water–snow–ice heat flux analogous to ground heat flux. Equations (1) and (2) are identical when solar radiation vanishes during nighttime. Specifically, the net ocean heat flux or ocean heat uptake is  $R_n - E - H$  equal to  $R_0 + Q$  according to Eq. (2). Note that solar radiation enters the surface energy balance equation through  $Q$ .

**(a) Land Surface Energy Budget**

**(b) Ocean Surface Energy Budget**


**Fig. 1** Surface energy balance equations over (a) land surfaces; (b) ocean (water–snow–ice) surface.  $R_S^{\downarrow}, R_S^{\uparrow}, R_L^{\downarrow}, R_L^{\uparrow}$  are downward shortwave, upward shortwave, downward longwave, upward longwave radiation;  $R_n$  the net radiation;  $E, H, Q$  the latent, sensible, and ground/surface water–snow–ice heat flux;  $R_0$  is the (net) solar radiation entering the (water–snow–ice) media. Radiation fluxes are positive (negative) when the surface receiving (emitting or reflecting). Thermal energy fluxes are positive when entering the atmosphere and/or surface media

An analytical expression of  $Q$  in terms of  $R_0$  and  $T_s$  is given in (Wang et al. 2014).

$R_n = E + H$ , the usually assumed global long-term surface energy budget, does not hold in general over sunlight transparent surfaces.  $R_n = E + H$  or  $R_0 + Q = 0$  implies that all solar radiation entering, e.g., ocean water, is transferred back into the atmosphere to balance ocean surface net long-wave radiation and turbulent heat fluxes as shown in Eq. (2). This is physically unrealistic since part of solar radiation absorbed by the water must dissipate through a number of physical, chemical and biological processes in the ocean including the thermal energy transport down to deeper ocean indicated by the decreasing ocean water temperature with depth (Liu et al. 2010; Kuhlbrodt and Gregory 2012), the conversion of thermal energy to kinetic energy for sustaining the global ocean general circulations (Laurent and Simmons 2006; Toggweiler and Samuels 1998), the energy consumed by chemical reactions such as photosynthesis (Behrenfeld and Falkowski 1997; Falkowski and Raven 2007; Pisciotta et al. 2010) among others. These previous studies suggested that the thermal energy responsible for the observed increasing ocean water temperature

[increasing ocean heat content, e.g., Levitus et al. (2012)], the quantity usually used to evaluate the imbalance between  $R_n$  and  $E + H$  (e.g., Stephens et al. 2012), is only a fraction of the solar radiation absorbed by the oceans.

Theoretically,  $R_n = E + H$  may not hold either over land surfaces. Even at annual (or longer) time scale, (quasi) steady-state of soil temperature does not necessarily lead to vanishing  $Q$ . The annual mean  $Q$  over land would be zero if (1) soil temperature has no trend at inter-annual timescales (no change of thermal energy storage), (2) annual mean soil heat flux at the bottom of the top soil layer vanishes, and (3) annual mean soil temperature profile is uniform, which rarely occurs (e.g., Gilichinsky et al. 1998; Qian et al. 2011; Bai et al. 2014) indicating that  $Q$  over land is likely non-zero at annual scale. The thermal energy entering the land surface ( $Q$ ) is transferred through several mechanisms not limited to heat conduction. For example, Heitman et al. (2008, 2010) showed that part of thermal energy entering the soil is used for subsurface evaporation (subsurface latent heat sink). The thermal energy in the soil may also be transferred downward by infiltrating rain water reaching groundwater aquifers much deeper than the top soil layer. Additionally, in situ measurements of  $Q$  could be underestimated by 18–66 % (in magnitude) due to the systematic negative bias of heat flux sensors (Ochsner et al. 2006).

## 2.2 Formulation of the MEP model

The MEP theory (Wang and Bras 2009) allows the turbulent latent heat  $E$ , sensible heat  $H$  and conductive heat flux  $Q$  over the Earth–atmosphere interface to be simultaneously solved in terms of analytical functions of surface radiation fluxes, temperature and/or humidity as the *most probable* partitioning of radiation fluxes while closing the surface energy budgets (satisfying the conservation of energy) by seeking an answer to the question “What is the best prediction of energy partitioning of surface radiation fluxes into surface heat fluxes based on the available surface energy and moisture states?”.

The MEP model formulation is described in (Wang and Bras 2011) for the case of land surfaces, and in (Wang et al. 2014) for the case of water–snow–ice surfaces due to different surface energy balance equations over solar radiation transparent and non-transparent media (soil vs. water–snow–ice) described in Eqs. (1)–(2). The MEP model predicted heat fluxes are expressed through the following algebraic equations by extremizing the dissipation (or entropy production) functions in Eqs. (7) (for land surfaces) and (12) (for water–snow–ice surfaces) (see “Appendix”) under the constraints of surface energy budgets as in Eqs. (1)–(2),

$$\left[ 1 + B(\sigma) + \frac{B(\sigma) I_s}{\sigma I_0} |H|^{-\frac{1}{6}} \right] H = R_n,$$

$$E = B(\sigma)H,$$

$$Q = \begin{cases} R_n - E - H & \text{land} \\ R_n^L - E - H & \text{water, snow, ice,} \end{cases} \quad (3)$$

$$B(\sigma) = 6 \left( \sqrt{1 + \frac{11}{36}\sigma} - 1 \right), \quad \sigma \equiv \frac{\lambda^2 q_s}{c_p R_v T_s^2}$$

where  $q_s$  is the surface (skin) specific humidity,  $T_s$  the surface (skin) temperature,  $\lambda$  the latent heat of vaporization of liquid/solid water,  $c_p$  the heat capacity of the air at constant pressure, and  $R_v$  the gas constant of water vapor.  $I_s$  the thermal inertia of the surface material (i.e., soil, leaf matrix of canopy, water, snow, and ice). For soil surface,  $I_s$  may be parameterized as a function of soil moisture (see “Appendix”). For canopy or dense forest land cover,  $I_s$  is negligible since the thermal inertia of leaf matrix is two orders of magnitudes smaller than that of soil.  $I_s$  of water, snow, and ice surfaces ( $=\sqrt{\rho c \lambda}$  with the density  $\rho$ , the specific heat  $c$ , and the thermal conductivity  $\lambda$  of water–snow–ice media) are  $1.56 \times 10^3$ ,  $0.6 - 1.4 \times 10^3$  (for snow density varied between 100 and 500 kg m<sup>-3</sup>), and  $1.92 \times 10^3$  J m<sup>-2</sup> K<sup>-1</sup> s<sup>-1/2</sup>, respectively.  $I_0$  is the “apparent” thermal inertia of the turbulent air as an eddy-diffusivity dependent parameter characterizing the boundary layer turbulence (see “Appendix”).

$B(\sigma)$  is recognized as the reciprocal Bowen ratio.  $\sigma$  is a dimensionless diagnostic parameter characterizing the relative role of surface humidity and temperature in the partitioning of the radiative fluxes. For the limiting case of dry soil, for example, vanishing  $\sigma$  ( $q_s = 0$ ) from zero soil moisture leads to  $E = 0$  (as  $B(\sigma) = 0$ ), i.e., the obvious solution of zero evaporation over dry soil. For the limiting case of saturated soil,  $q_s$  becomes the saturated specific humidity at  $T_s$  and  $\sigma$  becomes  $\Delta/\gamma$  with  $\Delta$  the slope of the saturation water vapor pressure curve at  $T_s$ , and  $\gamma$  the psychrometric constant. The corresponding  $E$  according to Eq. (3) is the potential evaporation by definition.

The surface heat fluxes  $E$ ,  $H$ , and  $Q$  can be solved from Eq. (3) given  $R_n$ ,  $T_s$ , and  $q_s$  data for the case of land surfaces and  $R_n$ ,  $R_n^L$ , and  $T_s$  data for the case of water, snow and ice surfaces. The MEP model only uses  $R_n$  and  $T_s$  data for the case of saturated land surfaces (e.g., saturated soils, irrigated farm lands and canopy under no water stress) where  $q_s$  is a function of  $T_s$  alone according to the Clausius–Clapeyron equation. Over water, snow, and ice surfaces,  $q_s$  is often assumed to be the saturation humidity at  $T_s$ . It can be shown that the solutions of  $E$ ,  $H$ , and  $Q$  from the nonlinear algebraic equations in Eq. (3) are unique.  $B$  in general is a function of  $q_s/T_s^2$  and of  $T_s$  only for saturated land and water–snow–ice surfaces. During nighttime, the

expressions of the MEP model over land and water–snow–ice surfaces are identical as  $R_n^S$  vanishes (i.e.,  $R_n = R_n^L$ ). Over water–snow–ice surface, the MEP  $E$  and  $H$  are solved from  $T_s$  and  $R_n$  only, while the MEP  $Q$  requires  $R_n^S$  or  $R_n^L$  ( $Q = R_n^L - E - H$ ) according to Eq. (3). In contrast, the MEP  $Q$  over land surfaces only needs input of  $R_n$  since soil is non-transparent to sunlight.

The MEP modeled fluxes as the partition of given radiation fluxes automatically close the surface energy budgets. As shown below, the uncertainties of the MEP modeled fluxes are dominated and bounded by the uncertainties of the surface radiation fluxes. The MEP model predicts heat fluxes without using temperature and humidity gradients, wind speed, and surface roughness data. However, *its independence of these variables should not be interpreted as temperature/humidity gradients, wind speed, and surface roughness playing no role in the corresponding transport processes*. The absence of these variables in the MEP formalism reflects strong and effective surface–atmosphere interactions so that the surface radiation fluxes together with surface temperature and/or humidity contain essential and sufficient information for the retrieval of the heat fluxes. Using the extremum solution of the Monin–Obukhov similarity equations (MOSE) (Wang and Bras 2010), temperature gradient and wind speed (or wind shear) are expressed as analytical functions of sensible heat and momentum fluxes, hence can be eliminated in the parameterization of eddy-diffusivity [through the “apparent” thermal inertia of the turbulent air  $I_0$  in Eq. (3)] in the MEP formalism. As is well understood, the use of roughness lengths in the formulation of transfer coefficients of the bulk transfer formulae based on the Monin–Obukhov similarity theory is a mathematical artefact. Roughness lengths are excluded from the variables in the MOSE derived using the Buckingham  $\pi$  theorem in the dimensional analysis (e.g., Arya 1988). They are only introduced by integrating the MOSE down to close-to-surface levels beyond the domain within which the premises underlying the MOSE hold.

The effect of horizontal advection of thermal energy, momentum and moisture on the surface energy budget is represented by the given surface variables  $R_n$ ,  $T_s$ , and  $q_s$  used in the MEP model. Therefore, the MEP method, as an inference algorithm as well as a physical principle, allows the heat fluxes to be retrieved using only radiation, temperature and/or humidity data. It is important to recognize that the MEP model parameterizes the same physical processes underlying the fluxes as those in the existing models including bulk transfer model. The difference is that the MEP method makes more effective use of the information most relevant to the heat fluxes provided by the surface variables (radiation, temperature, and/or humidity) than conventional methods.

### 2.2.1 Uncertainties of the MEP fluxes

The MEP model predicted fluxes as in Eq. (3) are mathematically expressed as functions of  $R_n$ , dimensionless variable  $\sigma \propto q_s/T_s^2$  and model parameter  $\beta \equiv I_d/I_0$ . The uncertainty of a flux  $X$  ( $X = E, H, Q$ ),  $\Delta X$ , may be expressed as, for the case of land surface,

$$\Delta X = \frac{\partial X}{\partial R_n} \Delta R_n + \frac{\partial X}{\partial \sigma} \Delta \sigma + \frac{\partial X}{\partial \beta} \Delta \beta, \quad (4)$$

where  $\Delta R_n$ ,  $\Delta \sigma$ , and  $\Delta \beta$ , are the uncertainties of  $R_n$ ,  $\sigma$ , and  $\beta$ , respectively, with  $\Delta \sigma$  and  $\Delta \beta$  related to the uncertainties of the physical variables  $\Delta T_s$ ,  $\Delta q_s$ , and parameters  $\Delta I_s$ ,  $\Delta I_0$  through,

$$\begin{aligned} \Delta \sigma &= \frac{\partial \sigma}{\partial T_s} \Delta T_s + \frac{\partial \sigma}{\partial q_s} \Delta q_s = \sigma \left( \frac{\Delta q_s}{q_s} - 2 \frac{\Delta T_s}{T_s} \right) \\ \Delta \beta &= \frac{\partial \beta}{\partial I_s} \Delta I_s + \frac{\partial \beta}{\partial I_0} \Delta I_0 = \beta \left( \frac{\Delta I_s}{I_s} - \frac{\Delta I_0}{I_0} \right) \end{aligned} \quad (5)$$

The partial derivatives in Eq. (4) are derived from Eq. (3),

$$\begin{aligned} \frac{\partial H}{\partial R_n} &= \left[ 1 + B + \frac{5B}{6\sigma} |H|^{-\frac{1}{6}} \right]^{-1} \\ \frac{\partial E}{\partial R_n} &= B \frac{\partial H}{\partial R_n} \\ \frac{\partial Q}{\partial R_n} &= 1 - \frac{\partial E}{\partial R_n} - \frac{\partial H}{\partial R_n} \\ \frac{\partial H}{\partial \sigma} &= H \left[ -\frac{11}{2(B+6)} + \frac{2B(B+6) - 11\sigma}{2\sigma(B+6)} \frac{\beta}{\sigma} |H|^{-\frac{1}{6}} \right] \\ &\quad \times \left[ 1 + B + \frac{5B}{6\sigma} |H|^{-\frac{1}{6}} \right]^{-1} \\ \frac{\partial E}{\partial \sigma} &= \frac{11}{2(B+6)} H + B \frac{\partial H}{\partial \sigma} \\ \frac{\partial Q}{\partial \sigma} &= -\frac{\partial E}{\partial \sigma} - \frac{\partial H}{\partial \sigma} \\ \frac{\partial H}{\partial \beta} &= -\frac{11}{2(B+6)} H |H|^{-\frac{1}{6}} \left[ 1 + B + \frac{5B}{6\sigma} |H|^{-\frac{1}{6}} \right]^{-1} \\ \frac{\partial E}{\partial \beta} &= B \frac{\partial H}{\partial \beta} \\ \frac{\partial Q}{\partial \beta} &= -\frac{\partial E}{\partial \beta} - \frac{\partial H}{\partial \beta} \end{aligned} \quad (6)$$

For the cases of water–snow–ice surfaces,  $\Delta q_s$  in Eq. (5) drops out as  $q_s$  over saturation surface is a function of  $T_s$ , while  $\Delta I_s = 0$  since the thermal inertia of still liquid water, snow and ice are known constants.  $\Delta \sigma$  is dominated by  $\Delta q_s$  due to relatively large uncertainty of humidity measurements ( $\Delta q_s/q_s \cong 10\%$  vs.  $\Delta T_s/T_s \cong 0.3\%$ ). In this study, uncertainty of  $I_0$  is ignored when the empirical coefficients in the MOSE are assumed to be known as fixed constants

(see “Appendix”). Then, the uncertainty of  $I_s$ , hence  $\beta$ , is caused by that of the thermal inertia of the soil materials  $I_d$  and soil moisture  $\theta$  according to Eq. (8). The uncertainty of  $I_s$  due to the measurement error of soil moisture  $\sim 0.04 \text{ m}^3 \text{ m}^{-3}$  is about 50 thermal inertia unit ( $\text{tiu} = \text{J m}^{-2} \text{ K}^{-1} \text{ s}^{-1/2}$ ) according to Eq. (8) (Yi et al. 2011; Lakshmi 2013). The dominant soil types of the Earth include sandy loam, loam, silt loam, sandy clay loam and clay loam (Nachtergaele et al. 2012) with thermal inertia in the range of 600–1000 tiu (Farouki 1982; Wang et al. 2010). In this analysis, a constant  $I_d = 800$  tiu is used as a representative value of  $I_d$ . Combing the two sources of uncertainties of  $I_s$  leads to a maximum  $\Delta I_s/I_s \cong 20\%$ . Note that  $I_s$  and the associated uncertainty only affect the MEP fluxes over two-third of the land masses not covered with dense forest.

### 2.2.2 Data

In this study, surface radiation and temperature data from NASA CERES during 2001–2010 are used as the input of the MEP model (Wielicki et al. 1996). The CERES is a set of radiometers designed based on the Radiation Budget Experiment (ERBE) (Barkstrom et al. 1989). The CERES data is derived from observations made by the Terra and Aqua satellites with improved spatial resolution and instrument calibration than previous generation of ERBE products. The surface radiation from the CERES SYN 1 deg-3Hour data product (Edition 3A, Level 3) with 3-hourly  $1^\circ \times 1^\circ$  resolution is used (<http://ceres.larc.nasa.gov/products.php?product=SYN1deg>). The CERES SYN1 deg-3Hour surface radiative fluxes are computed based on the Langley Fu-Liou radiative transfer model (Fu and Liou 1993) using the cloud properties from Moderate Resolution Imaging Spectroradiometer (MODIS) and geostationary (GEO) satellite, atmospheric profiles from Global Modeling and Assimilation Office (GMAO), and aerosol properties from MODIS. The modeled radiative fluxes are constrained (tuned) to the observed CERES top-of-atmosphere fluxes. The CERES surface temperature data are obtained using the GMAO Goddard Earth Observing System Model (GEOS). The uncertainty of CERES global, land, and ocean annual surface net radiation (12, 16, and  $14 \text{ W m}^{-2}$ , respectively) is estimated based on the observations of cloud and aerosols properties from Cloud–Aerosol Lidar and Infrared Pathfinder Satellite Observations (CALIPSO), CloudSat, and MODIS (Kato et al. 2012). They will be used in the uncertainty analysis of the MEP fluxes in this study.

Surface specific humidity and top layer soil moisture over the same period are available from the NASA MERRA reanalysis dataset with hourly  $0.5^\circ \times 0.67^\circ$  resolution (Bosilovich et al. 2011; Rienecker et al. 2011) (<http://disc.sci.gsfc.nasa.gov/daac-bin/DataHoldings.pl>). The ocean surface (conductive) heat flux is computed as the

residual of the energy balance equation as in Eq. (2) since it is not available from the MERRA product (and other reanalysis data products). Land-cover data are from the International Geosphere-Biosphere Programme (IGBP) data set with  $1/60^\circ$  resolution (Townshend 1992) (<http://modis-atmos.gsfc.nasa.gov/ECOSYSTEM/format.html>). All the input variables of the MEP model are converted to 3-hourly  $1^\circ \times 1^\circ$  resolution.

### 3 Results

Tests of the MEP model using field observations reported previously by the model developers (Wang and Bras 2009, 2011; Wang et al. 2014) provide evidence that the MEP model is able to predict the surface heat fluxes of both land and water–snow–ice surface at field scales. Independent tests of the MEP model have also been reported (e.g., Nearing et al. 2012; Yang and Wang 2014; Shanafield et al. 2015) showing that the MEP model matches or outperforms other existing models. These early applications of the MEP model justify its potential as an alternative approach for modeling the surface heat fluxes at regional and global scales.

Figure 2a shows the MEP model predicted 2001–2010 climatology of evapotranspiration or latent heat flux  $E$  (top panel) over land using the 3-hourly CERES net radiation and surface temperature data supplemented by the MERRA surface specific humidity and soil moisture. The MEP annual mean  $E$ ,  $480 \text{ mm year}^{-1}$  ( $1.31 \text{ mm day}^{-1}$  or  $38 \text{ W m}^{-2}$ ), is consistent with earlier estimates including, for example,  $467 \text{ mm year}^{-1}$  ( $37 \text{ W m}^{-2}$ ) from the NASA Global Land Data Assimilation System (GLDAS) reanalysis data (Rodell et al. 2004; Wang and Dickinson 2012), the 1982–2008 climatology  $478 \text{ mm year}^{-1}$  (Jung et al. 2010) based on the analysis combining global ground fluxes network (Fig. 2c), satellite remote sensing with surface meteorological data but lower than  $642 \text{ mm year}^{-1}$  from the MERRA reanalysis data (Fig. 2b) although with similar spatial patterns. The MEP global annual mean  $E$  is also comparable to other existing reports and data products shown in Table 1. Other reported estimates, e.g., Figure 1(a) in (Mueller et al. 2011), Table 8 in (Wang and Dickinson 2012), range from  $303 \text{ mm year}^{-1}$  ( $0.83 \text{ mm day}^{-1}$  or  $24.1 \text{ W m}^{-2}$ ) to  $730 \text{ mm year}^{-1}$  ( $2 \text{ mm day}^{-1}$  or  $58 \text{ W m}^{-2}$ ). The uncertainty of the global annual mean of the MEP  $E$  over land mass is  $126 \text{ mm year}^{-1}$  ( $0.35 \text{ mm day}^{-1}$  or  $10 \text{ W m}^{-2}$ ) calculated using Eqs. (4)–(6) at the global annual mean fluxes given in Table 1.

Table 2 provides the representative values of the partial derivatives and model input/parameter uncertainties of MEP heat fluxes as in Eq. (4) and the relative contributions of  $R_n$ ,  $\sigma$ , and  $\beta$  to the MEP fluxes. 57 % of the

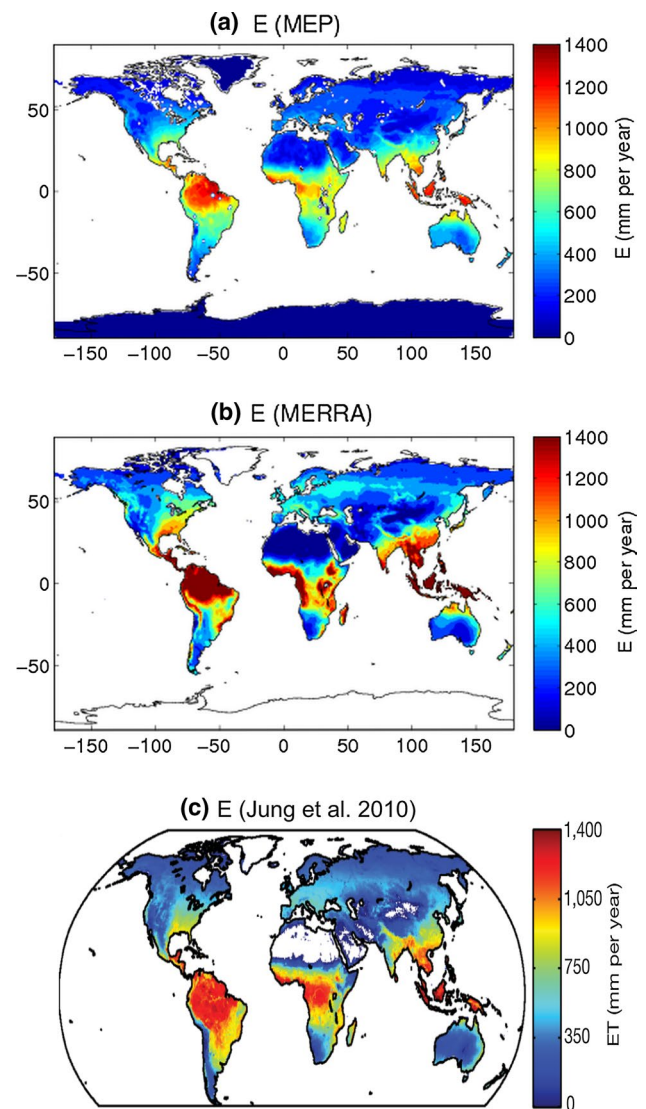


**Fig. 2** a MEP model predicted annual mean  $E$  (2001–2010) according to Eq. (3) using the 3-hourly CERES SYN1 deg-3Hour net radiation, GMAO GEOS surface temperature, and the MERRA reanalysis surface specific humidity data; b MERRA data of annual mean  $E$  (2001–2010); c annual mean  $E$  (1982–2008) based on FLUXNET, satellite remote sensing and surface meteorological data (Jung et al. 2010)

uncertainty of MEP modeled  $E$  over land is attributed to that of the net radiation data, 27 % to the parameter  $\sigma$  representing the uncertainties from temperature and humidity data, 16 % to the thermal inertia parameter  $\beta$  (see Table 2). We emphasize that the MEP modeled  $E$  is obtained using fewer input data and model parameters than those of the existing models and balances the surface energy budget. The global annual mean  $E$  over land has an increasing trend of  $5.05 \text{ mm year}^{-1} \text{ year}^{-1}$  ( $0.4 \text{ W m}^{-2} \text{ year}^{-1}$ ) during 2001–2010 with the 95 % confidence interval (CI) estimated as  $2.78 \text{ mm year}^{-1} \text{ year}^{-1}$  ( $0.22 \text{ W m}^{-2} \text{ year}^{-1}$ ).

**Table 1** The global climatology of the MEP modeled surface heat fluxes ( $W\ m^{-2}$ ) according to Eq. (3) and products from Global Land Data Assimilation System (GLDAS), Objectively Analyzed Air–Sea Fluxes (OASFlux), NCEP/NCAR reanalysis, NCEP/DOE II reanalysis, and Japanese reanalysis (JRA); Hamburg Ocean Atmosphere Parameters and Fluxes from Satellite Data (HOAPS), SeaFlux data, and other published studies

Global	$E$	$H$	$Q$	$R_n$	$R_n^L$	$R_n - E - H (= R_0 + Q)$
MEP	53 ± 6	30 ± 4	–	114 ± 12	–57 ± 10	31 ± 5
Stephens et al. (2012)	88 ± 10	24 ± 7	–	113 ± 15	–57 ± 14	1
Trenberth et al. (2009)	80	17	–	98	–63	0
MERRA (2001–2010)	81	23	–	111	–66	7
NCEP/NCAR <sup>1</sup>	81	16	–	100	–61	3
NCEP/DOE II <sup>1</sup>	91	8	–	103	–57	4
CFSR <sup>1</sup>	84	16	–	110	–57	10
JRA <sup>2</sup>	90	19	–	97	–73	–12
<b>Land</b>						
MEP	38 ± 10	33 ± 7	12 ± 10	84 ± 16	–69 ± 11	–*
Trenberth et al. (2009)	39	27	0 <sup>a</sup>	66	–80	–*
MERRA (2001–2010)	51	41	0 <sup>a</sup>	92	–74	–*
GLDAS (2001–2010)	37	51	0.5	88	–65	–*
NCEP/NCAR <sup>1</sup>	51	26	3 <sup>a</sup>	80	–73	–*
NCEP/DOE II <sup>1</sup>	52	13	7 <sup>a</sup>	72	–71	–*
CFSR <sup>1</sup>	38	35	0 <sup>a</sup>	74	–66	–*
JRA <sup>2</sup>	39	27	2 <sup>a</sup>	69	–87	–*
Jiménez et al. (2011)	45 ± 15	45 ± 15	0 <sup>a</sup>	90 ± 15	–	–*
Mueller et al. (2011)	48 ± 6	–	–	–	–	–
Mueller et al. (2013)	39 ± 12	–	–	–	–	–
Wang and Dickinson (2012)	35 ± 9	–	–	–	–	–
Vinukollu et al. (2011)	42 ± 5	–	–	–	–	–
Yuan et al. (2010)	33 ± 3	–	–	–	–	–
Zhang et al. (2010)	43	–	–	–	–	–
<b>Ocean</b>						
MEP	58 ± 7	28 ± 3	–139 ± 10	125 ± 14	–52 ± 12	39 ± 4
Trenberth et al. (2009)	97	12	–166 <sup>b</sup>	110	–57	1
MERRA (2001–2010)	92	16	–171 <sup>b</sup>	118	–63	10
OASFlux (2001–2010)	98 ± 7	10 ± 1	–161 <sup>b</sup>	134	–52	25
NCEP/NCAR <sup>1</sup>	94	11	–161 <sup>b</sup>	109	–56	4
NCEP/DOE II <sup>1</sup>	106	6	–163 <sup>b</sup>	116	–51	4
CFSR <sup>1</sup>	103	9	–166 <sup>b</sup>	124	–54	12
JRA <sup>2</sup>	109	17	–194 <sup>b</sup>	107	–68	–19
HOAPS <sup>2</sup>	104 ± 10	15	–	–	–	–
SeaFlux <sup>3</sup>	90 ± 14	18 ± 6	–	–	–	–

$R_o = R_s^↓ - R_s^↑$  is defined in Eq. (2)

\*  $R_n - E - H = Q$  over land surfaces

<sup>a</sup>  $Q$  calculated as the residual of the energy balance equation as in Eq. (1)

<sup>b</sup>  $Q$  calculated as the residual of the energy balance equation as in Eq. (2)

<sup>1</sup> Wang et al. (2011)

<sup>2</sup> Trenberth et al. (2009)

<sup>3</sup> Clayson et al. (2014)

The increasing trend of MEP  $E$  results from the increasing trends of CERES  $R_n$  and MERRA  $q_s$  as shown in Fig. 3, while Jung et al. (2010) reported a decreasing trend of the

global annual mean  $E$  due to the negative trend of global soil moisture during 1998–2008 derived from the Tropical Rainfall Measuring Mission’s (TRMM) (Owe et al. 2008).

**Table 2** The representative values of (a) the partial derivatives and uncertainties of variables in Eq. (3) calculated at the annual mean radiation fluxes, temperature and humidity data; (b) relative contributions of uncertainties of the independent variables  $R_n$ ,  $\sigma$ , and  $\beta$  to the uncertainties of the MEP fluxes according to Eqs. (4)–(6)

Global	$ \partial X/\partial R_n $	$\Delta R_n$	$ \partial X/\partial \sigma $	$\Delta \sigma$	$ \partial X/\partial \beta $	$\Delta \beta$
(a)						
$E$	0.44		12.82		5.39	
$H$	0.26	12	4.97	0.05	3.14	0.07
$R_n - E - H (= R_0 + Q)$	0.3		17.77		8.53	
Land						
$E$	0.35		17.06		4.80	
$H$	0.31	16	6.93	0.15	4.33	0.32
$Q$	0.35		10.10		9.13	
Ocean						
$E$	0.47		11.26		5.23	
$H$	0.24	14	4.26	0.02	2.72	0
$Q$	0.71		7.00		7.95	
Global		$R_n$		$\sigma$		$\beta$
(b)						
$E$		83		11		6
$H$		86		7		6
$R_n - E - H (= R_0 + Q)$		71		17		12
Land						
$E$		57		27		16
$H$		67		14		19
$Q$		55		16		29
Ocean						
$E$		97		3		0
$H$		98		2		0
$Q$		99		1		0

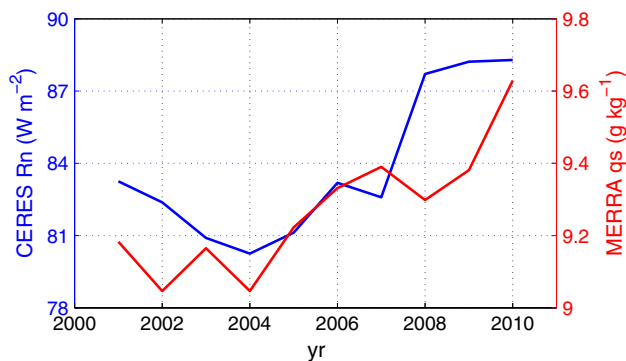


**Fig. 3** Global annual mean of CERES  $R_n$  (left y axis) and MERRA  $q_s$  (right y axis) over land during 2001–2010

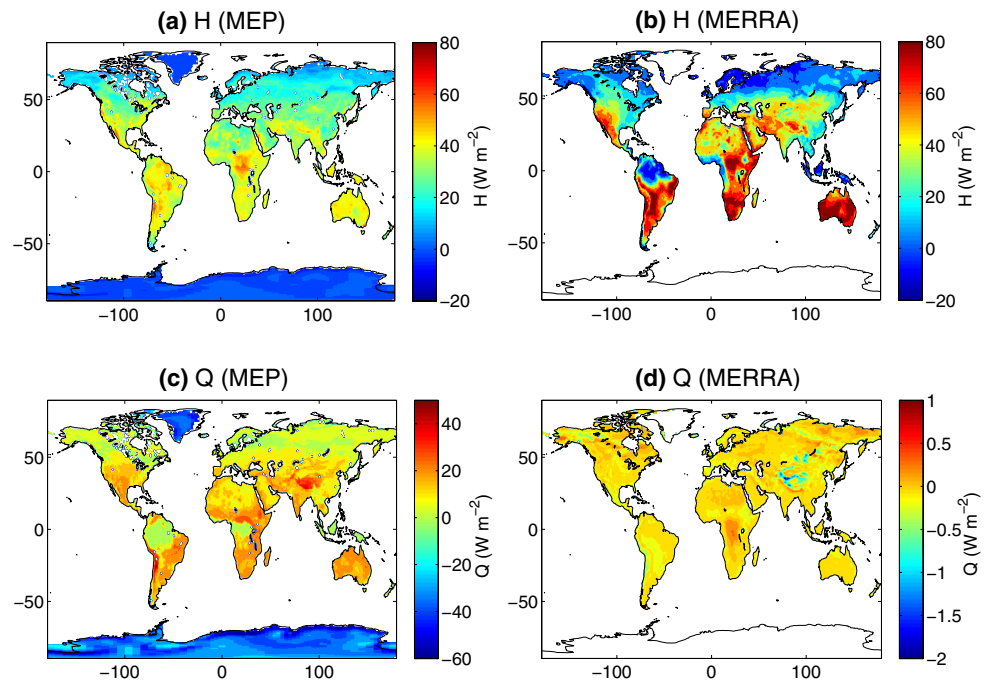
Greater  $R_n$  and  $q_s$  lead to higher  $E$  according to the MEP model. Higher  $R_n$  implies more radiation energy, while higher  $q_s$  favors radiation energy dissipated through latent heat of phase change.

Figure 4 shows the MEP modeled global annual mean  $H$  and  $Q$  over land compared with the MERRA reanalysis data. It is evident that the spatial pattern of the MEP modeled  $H$  is consistent with the corresponding MERRA data. The MEP global annual mean  $H$ ,  $33 \text{ W m}^{-2}$ , agrees with several earlier estimates (Table 1), but lower than GLDAS ( $51 \text{ W m}^{-2}$ ) and MERRA ( $41 \text{ W m}^{-2}$ ) products. Noticeable differences between the MEP and GLDAS annual mean  $H$  (not shown) occur over Greenland where the MEP model predicts small ( $<10 \text{ W m}^{-2}$ ) and positive  $H$ , while the GLDAS  $H$  is  $\sim 30 \text{ W m}^{-2}$ . The uncertainty of the MEP modeled global annual mean  $H$ ,  $7 \text{ W m}^{-2}$  (Table 1), is attributed to that of  $R_n$  (67 %),  $\sigma$  (14 %), and  $\beta$  (19 %) as shown in Table 2. The MEP global annual mean  $H$  has an increasing trend of  $0.18 \text{ W m}^{-2} \text{ year}^{-1}$  (not shown) associated with the increasing trend of the CERES  $R_n$  (Fig. 3). The uncertainty of the trend was estimated as  $0.18 \text{ W m}^{-2} \text{ year}^{-1}$ .

The MEP model predicts a global annual mean  $Q$  of  $12 \text{ W m}^{-2}$  over land shown in Fig. 4 and Table 1. The



**Fig. 4** The MEP modeled a sensible heat flux  $H$ ; **b** MERRA  $H$ ; **c** MEP modeled ground heat flux  $Q$ ; **d** MERRA  $Q$ . The MEP modeled  $H$  and  $Q$  are obtained according to Eq. (3) using the 3-hourly CERES SYN1 deg-3Hour surface net radiation and surface temperature, and the MERRA surface specific humidity data. All fluxes are annual means over 2001–2010



spatial distribution of the MEP modeled  $Q$  depends on land cover with vanishing  $Q$  over dense canopy covered areas including the Amazonia, high latitude North America and Eurasian continent. Negative  $Q$  over Greenland is physically realistic since the thermal energy from the absorption of solar radiation is transferred from snow-ice layer into the atmosphere. 55, 16, and 29 % of the  $10 \text{ W m}^{-2}$  uncertainty of the global annual mean  $Q$  are caused by the uncertainty of  $R_n$ ,  $\sigma$ , and  $\beta$ , respectively.

$12 \text{ W m}^{-2}$  global annual mean  $Q$  over land using the 3-hourly CERES data of net radiation and surface temperature is likely over-estimated due to the effect of the temporal resolution of the data. A sensitivity analysis (Huang et al. 2014) on the effect of the temporal resolution of input data on the MEP fluxes using field observations showed that using daily data in the MEP model tends to over-estimate daily  $Q$  by one-third compared to that using half-hourly data. The land mass gaining thermal energy at the annual scale predicted by the MEP model is consistent with the NCEP reanalysis (Table 1), while the MERRA and GLDAS reanalysis products have nearly zero annual mean  $Q$  ( $<1 \text{ W m}^{-2}$  in Table 1). The MEP modeled global annual mean  $Q$  has an increasing trend of  $0.20 \text{ W m}^{-2} \text{ year}^{-1}$  associated with the increasing trend of the CERES  $R_n$ . The 95 % CI of the trend was estimated as  $0.18 \text{ W m}^{-2} \text{ year}^{-1}$ .

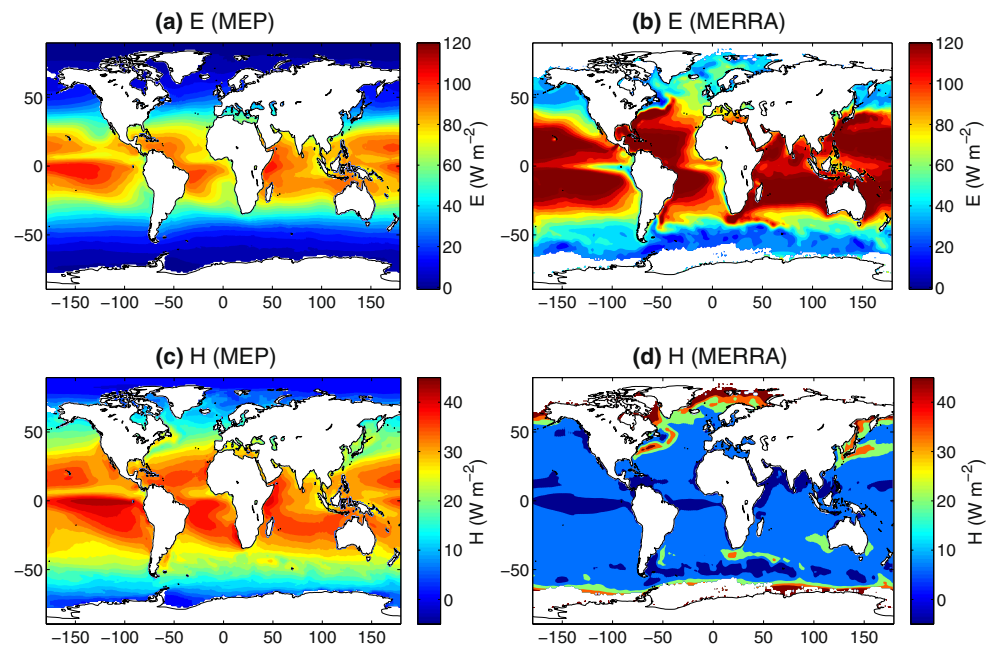
The zero global annual mean  $Q$  estimated by MERRA is likely underestimated presumably caused by the underestimated soil temperature gradient. In the MERRA land surface scheme,  $Q$  is linearly proportional to the near surface temperature gradient (Pan and Mahrt 1987). However, the “surface temperature” in the MERRA land surface scheme

to compute temperature gradient is the soil temperature of the top soil layer (0–5 cm) instead of “skin” temperature (Koster et al. 2000). As a result, the surface soil temperature gradient in MERRA is underestimated given the sharp gradient of soil temperature near the surface, leading to underestimated  $Q$ .

Figure 5 shows the MEP modeled annual mean  $E$  and  $H$  over oceans using the 3-hourly CERES radiation fluxes and sea surface temperature (SST) data for the period 2001–2010 compared with the MERRA data. The spatial pattern of the MEP  $E$  is consistent with the MERRA data, while the spatial pattern of the MEP  $H$  is substantially different from the MERRA data. The spatial patterns of the MEP  $E$  and  $H$  are consistent with that of the CERES  $R_n$ . The MEP estimated  $E$  and  $H$  are constrained by  $R_n$ , while the MERRA estimated  $E$  and  $H$  over several regions such as western and northern Pacific and Atlantic oceans are unrealistically large (greater than  $R_n$ , which violates the conservation of energy). The MEP  $E$  is lower than the MERRA  $E$  in most of areas, while the MEP  $H$  is in general greater than the MERRA  $H$  as shown in Fig. 5.

Previous studies showed that the MERRA  $E$  and  $H$  are subject to large uncertainty caused by the biases of model inputs, especially wind and vertical temperature/humidity gradient (Brunke et al. 2011; Roberts et al. 2012). The large uncertainty in the MERRA data makes it difficult to validate the discrepancy between the MEP and MERRA estimates. Roberts et al. (2012) compared the MERRA  $E$  and  $H$  over oceans with directly measured  $E$  and  $H$  and other observational-based datasets (satellite-based and pseudo-observational flux product). They found that the MERRA  $E$  is

**Fig. 5** The 2001–2010 climatology of the MEP modeled annual mean latent  $E$  and sensible  $H$  heat fluxes over ocean (left panel) derived using the 3-hourly surface net radiation and net long-wave radiation from CERES SYN1 deg-3Hour data and sea surface temperature (SST) from GMAO GEOS versus the MERRA reanalysis data (right panel)

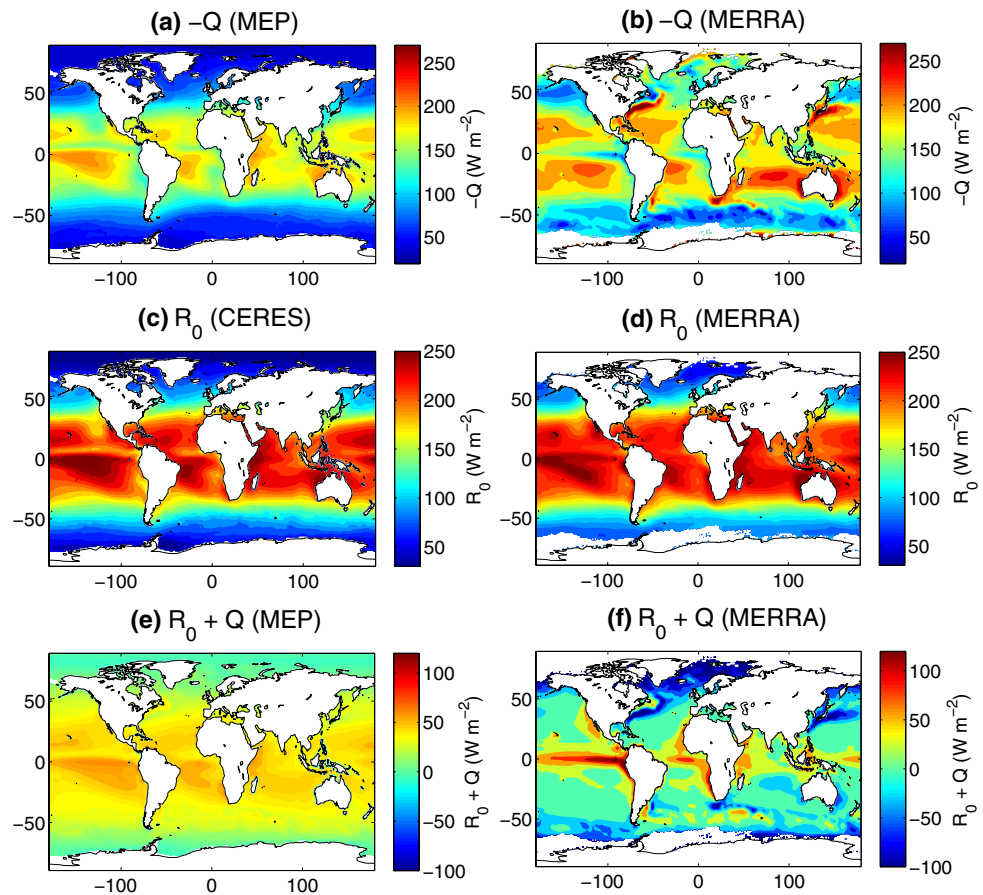


generally overestimated, while the MERRA  $H$  is often underestimated. The overestimates of MERRA  $E$  mainly result from the positive biases of wind speed and vertical humidity gradient. The underestimation of MERRA  $H$  compared to observations is primarily caused by the corresponding negative bias of vertical temperature gradient, while the areas with high  $H$  are presumably due to the large positive wind bias. They also found that the MERRA  $E$  and  $H$  have variable biases corresponding to different regimes of observed heat fluxes. MERRA overestimates  $E$  about  $25 \text{ W m}^{-2}$  when the observed  $E$  below  $50 \text{ W m}^{-2}$ , while MERRA underestimates  $E$  up to  $100 \text{ W m}^{-2}$  when the observed greater than  $250 \text{ W m}^{-2}$ . For most densely observed regions from  $50$  to  $100 \text{ W m}^{-2}$ , the MERRA  $E$  is overestimated about  $10 \text{ W m}^{-2}$ . MERRA overestimates  $H$  by  $50$ – $75 \%$  when observations are less than  $-15 \text{ W m}^{-2}$ , however, MERRA underestimates  $H$  by  $20$ – $50 \text{ W m}^{-2}$  when observed  $H$  greater than  $40 \text{ W m}^{-2}$ .

The MEP global annual mean ocean fluxes versus some previous estimates are summarized in Table 1. The MEP modeled annual mean  $E$  over oceans is  $733 \pm 88 \text{ mm year}^{-1}$  ( $58 \pm 7 \text{ W m}^{-2}$ ), which is lower than the previous estimates in the range of  $1130$ – $1370 \text{ mm year}^{-1}$  ( $90$ – $109 \text{ W m}^{-2}$ ). The MEP model estimated  $H$  is  $28 \pm 3 \text{ W m}^{-2}$ , which is higher than the previous estimates of  $\sim 10$ – $20 \text{ W m}^{-2}$ . The MEP estimated  $E$  and  $H$  have decreasing trends of  $-0.05$  and  $-0.03 \text{ W m}^{-2} \text{ year}^{-1}$  associated with an decreasing trend of  $R_n^L$ . The uncertainties of the trends of MEP  $E$  and  $H$  were estimated as  $0.06$  and  $0.04 \text{ W m}^{-2} \text{ year}^{-1}$ , respectively. Note that the MEP annual mean  $E + H$ ,  $86 \text{ W m}^{-2}$ , is not equal to the CERES annual mean  $R_n$ ,  $125 \text{ W m}^{-2}$  with a positive net ocean heat flux (ocean heat uptake)  $R_n - E - H$ , for the reason discussed in Sect. 2.

The MEP model gives the first directly modeled global ocean surface heat flux  $Q$  as shown in Fig. 6a (positive  $-Q$  indicates that thermal energy is transferred from the ocean to the atmosphere). Note that  $Q$  is not available from existing data products including MERRA, NCEP, and European Centre for Medium-Range Weather Forecasts (ECMWF) reanalysis products. For the purpose of comparison, the MERRA annual mean  $Q$  shown in Fig. 6b is calculated as the residual of the ocean surface energy balance equation as in Eq. (2) where  $E$ ,  $H$ , and  $R_n^L$  data are from the MERRA reanalysis product. The spatial pattern of MEP  $Q$  is largely consistent with the MERRA based  $Q$ . The MEP global annual mean  $Q$  is about  $-139 \pm 10 \text{ W m}^{-2}$ , which is  $15$ – $20 \%$  lower than the other data products (also derived as the residual of the energy balance equation) as shown in Table 1. The MEP  $Q$  over the global oceans has a decreasing trend of  $-0.09 \text{ W m}^{-2} \text{ year}^{-1}$  during 2001–2010 with uncertainty of  $0.16 \text{ W m}^{-2} \text{ year}^{-1}$ . Also shown in Fig. 6c–f are the CERES and MERRA ocean surface net solar radiation  $R_o$  and net ocean heat flux  $R_o + Q = R_n - E - H$ , which are consistent with that of  $R_n$ , but substantially differs from the MERRA based estimates. Nevertheless, the positive  $R_o + Q$  predicted by the MEP model ( $39 \pm 4 \text{ W m}^{-2}$ ) indicates that the oceans gain thermal energy at the annual scale, which is qualitatively in agreement with previous estimates ranging from  $3$  to  $33 \text{ W m}^{-2}$  (Yu and Weller 2012) and most of data products listed in Table 1 except for the Japan reanalysis (JRA). Yet we argue that non-zero  $R_o + Q$  is a physical reality rather than a numerical artefact due to modeling errors and uncertainties of model parameters as discussed above. Quantitative analysis of energy dissipation in the oceans is needed but beyond the scope of

**Fig. 6** The 2001–2010 climatology of the (a) MEP modeled annual mean ocean surface heat flux  $Q$  ( $-Q$  is shown), (c) net solar radiation  $R_0$ , and (e) net ocean heat flux (ocean heat uptake)  $R_0 + Q$  ( $R_n - E - H$ ) derived using the same input data as in Fig. 5 versus the corresponding MERRA reanalysis data (right panel)



this study. The uncertainties of the global annual mean of MEP heat fluxes over oceans are dominated by the uncertainty of  $R_n$  measurements ( $\geq 97\%$ ).

The MEP modeled global annual mean fluxes are summarized in Table 1. The newly estimated global annual mean  $E$ ,  $53 \pm 6 \text{ W m}^{-2}$ , is lower than previous estimates of  $80\text{--}90 \text{ W m}^{-2}$  largely due to the lower MEP  $E$  over oceans. The new estimate of annual mean  $H$  is  $30 \pm 4 \text{ W m}^{-2}$ , while previously reported annual mean  $H$  has a range of  $8\text{--}24 \text{ W m}^{-2}$ . The MEP estimate of global annual net surface heat flux is  $\sim 31 \pm 5 \text{ W m}^{-2}$ , while previous reanalysis products all have nearly zero annual ground/water–snow–ice heat flux.

Since direct measurements of heat fluxes over oceans are limited, the MEP fluxes may be validated indirectly by comparing the net ocean heat flux with the change of ocean heat content ( $\Delta OHC$ ) of the top ocean layer of certain depth as  $\Delta OHC$  is expected to be positively correlated with  $R_n - E - H$ . Figure 7 shows that the MEP modeled global annual mean  $R_n - E - H$  has a decreasing trend during 2001–2010 qualitatively consistent, as expected, with the decreasing trend of the  $\Delta OHC$  of the top 700-m layer from the National Climatic Data Center (NCDC) data (Levitus et al. 2012). One explanation for the large values

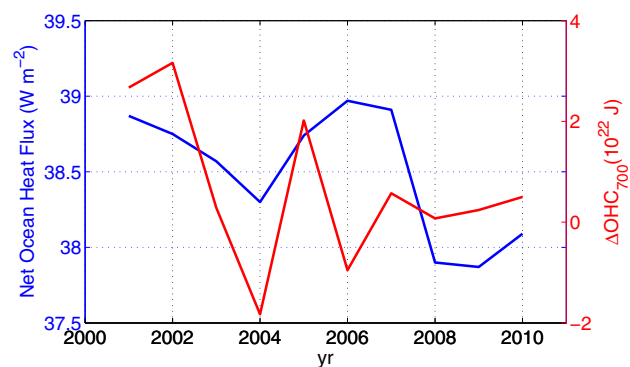


**Fig. 7** The annual mean MEP modeled net ocean heat flux (ocean heat uptake)  $R_n - E - H$  versus the change in the top 700 m ocean heat content ( $\Delta OHC$ ) from NCDC. The correlation between  $R_n - E - H$  and  $\Delta OHC$  is 0.4

MEP  $R_n - E - H$  relative to  $\Delta OHC$  is that part of the absorbed solar radiation by the oceans is transferred into deeper ocean layers and dissipated through other physical, chemical and biological processes within the oceans.

The MEP modeled fluxes have reduced uncertainties compared to the existing data products as the bulk gradients of temperature/humidity gradients, wind speed, and

surface roughness lengths subject to large uncertainties are excluded from the MEP model. The uncertainties of MEP fluxes are mainly caused by the uncertainties of the surface radiation data as shown in Table 2. The model parameter caused uncertainties of the MEP fluxes are limited compared to previous estimates using the conventional methods (Mueller et al. 2011, 2013; Vinukollu et al. 2011; Stephens et al. 2012; Yuan et al. 2010; Yu et al. 2008; Bourras 2006; Clayson et al. 2014). The uncertainties of the MEP estimated heat fluxes can be further reduced with the improved accuracy of radiation measurements in the future.

## 4 Conclusion

The MEP model produces new estimates of global annual mean evaporation rate of  $667 \text{ mm year}^{-1}$  ( $\pm 76 \text{ mm year}^{-1}$ ), sensible heat flux of  $30 \text{ W m}^{-2}$  ( $\pm 4 \text{ W m}^{-2}$ ), ground (conductive) heat flux (over land) of  $12 \text{ W m}^{-2}$  ( $\pm 10 \text{ W m}^{-2}$ ) and ocean surface heat flux of  $139 \text{ W m}^{-2}$  ( $\pm 10 \text{ W m}^{-2}$ ) (through conductive cool-skin). The MEP estimate of the net ocean heat flux (or ocean heat uptake) is  $39 \text{ W m}^{-2}$  ( $\pm 4 \text{ W m}^{-2}$ ). The new estimate of terrestrial evapotranspiration based on the MEP model is in close agreement with previous estimates while the estimate of ocean evaporation is lower than bulk flux based estimates. The MEP model produces the first estimate of global ocean surface heat flux that is not available from existing data products.

The MEP modeled surface heat fluxes not only (by definition) close surface energy budgets at all space–time scales, but also avoid explicit uses of temperature/moisture gradients, wind speed and surface roughness as model inputs and parameters. These unique properties make the MEP model a potentially powerful tool facilitating the monitor and evaluation of regional and global surface water and energy budgets, especially over sparsely instrumented polar regions, sea ice surfaces, and remote continental areas. The MEP model may serve as an effective physical parameterization of the land–ocean–atmosphere interaction in regional and global numerical weather prediction and climate models, contributing to the study of changes of water–energy–carbon cycles in response to radiative forcing perturbations of both natural and anthropogenic origins. The discrepancies between the MEP-based heat flux estimates and those based upon more traditional approaches arise from multiple sources including uncertainties from both input variables and model parameters. These issues are further exacerbated by difficulties in obtaining “ground-truth” measurements of heat fluxes over oceans and significant uncertainties in deriving surface radiative fluxes through radiative transfer calculations (e.g., in the presence of clouds). Constructing a new global surface energy budget and putting the MEP model results in a broader perspective of the climate system’s energy cycle

is the first step of our ongoing efforts. New results will be reported in the near future.

**Acknowledgments** This study is sponsored by National Aeronautics and Space Administration NEWS program Grant NNX15AT41G. Partial support was provided by National Science Foundation Grants EAR-1331846 and EAR-1138611, National Science Foundation Grants AGS-1354402 and AGS-1445956.

## Compliance with ethical standards

**Conflict of interest** The authors declare that they have no conflict of interest.

## Appendix: Dissipation functions and thermal inertia parameters

For the case of land surface (non-transparent media), the dissipation function  $D$  is expressed as the function of latent  $E$ , sensible  $H$  and ground  $Q$  heat flux (Wang and Bras 2011),

$$D(E, H, Q) \equiv \frac{2Q^2}{I_s} + \frac{2E^2}{I_e} + \frac{2H^2}{I_a}, \quad (7)$$

where  $I_s$ ,  $I_e$  and  $I_a$  are the thermal inertia parameters ( $\text{J m}^{-2} \text{K}^{-1} \text{s}^{-1/2}$ ) associated with the corresponding fluxes. Thermal inertia of soil  $I_s$  may be parameterized using an empirical equation,

$$I_s = \sqrt{I_d^2 + \theta I_w^2}, \quad (8)$$

where  $\theta$  is the volumetric water content,  $I_d$  the thermal inertia of dry soil, and  $I_w$  the thermal inertia of (still) liquid water.  $I_a$  and  $I_e$  characterizing turbulent transport of heat and water vapor in the boundary layer are parameterized based on the Monin–Obukhov similarity theory (Wang and Bras 2010, 2011),

$$I_a = I_0 |H|^{1/6}, \quad I_e = \sigma I_a, \quad (9)$$

where  $\sigma$  given in Eq. (3) is a dimensionless coefficient characterizing the thermal and moisture condition on the partition of radiation energy.  $I_0$  is the “apparent” thermal inertia of the turbulent air representing the turbulent transport processes in the boundary layer.  $I_0$  in Eqs. (3) and (9) was formulated using the extremum solution of the Monin–Obukhov similarity equations (Wang and Bras 2009) as,

$$I_0 = C_0 \rho_a c_p \sqrt{\kappa z} \left( \frac{\kappa g z}{\rho_a c_p T_0} \right)^{1/6}, \quad (10)$$

with a universal empirical constant  $C_0$  related to the coefficients in the dimensionless functions characterizing the atmospheric stability (Businger et al. 1971),

$$C_0 = \begin{cases} 1.7 & \text{Unstable} \\ 1.2 & \text{Stable} \end{cases}, \quad (11)$$

where  $\rho_a$  is the density of air,  $\kappa = 0.4$  the von Kármán constant,  $T_0$  (~300 K) a representative environment temperature, and  $g$  the gravitational acceleration.  $z$  is the distance from the material surface above which the Monin–Obukhov similarity equations hold. Based on the tests over the land surfaces,  $z$  may be chosen as 2–3 m for the case of flat bare soil, 4–5 m for the case of short vegetation, and 9–10 m for the case of tall trees. In this study,  $z$  for the case of oceans is set at 2.5 m above which the sensitivity of the MEP model predicted heat fluxes on  $z$  is weak.

For the cases of water, snow, and ice surfaces (transparent media),  $D$  is expressed as the function of latent  $E$ , sensible  $H$  and (conductive) water/snow/ice surface  $Q$  heat flux (Wang et al. 2014),

$$D(E, H, Q) \equiv \frac{2(Q + R_n^S)^2}{I_s} + \frac{2E^2}{I_e} + \frac{2H^2}{I_a}, \quad (12)$$

where  $R_n^S$  is the surface net solar radiation,  $I_s$  the thermal inertia of (still) liquid water, snow or ice, and  $I_a$  and  $I_e$  are identical to those in Eq. (9) for the case of land surface.

## References

- Arya S (1988) Introduction to micrometeorology. Academic Press, New York
- Badgley F (1966) Heat balance at the surface of the Arctic Ocean. Symposium on the arctic heat budget and atmospheric circulation. In: Proceedings; Rand Corporation. Research memorandum. RM-5233-NSF
- Bai Y, Scott T, Min Q (2014) Climate change implications of soil temperature in the Mojave Desert, USA. *Front Earth Sci* 8(2):302–308. doi:10.1007/s11707-013-0398-3
- Barkstrom B, Harrison E, Smith G, Green R, Kibler J, Cess R, The ERBE Science Team (1989) Earth radiation budget experiment (ERBE) archival and April 1985 results. *Bull Am Meteorol Soc* 70:1254–1262. doi:10.1175/1520-0477(1989)070<1254:ERBEA>2.0.CO;2
- Behrenfeld M, Falkowski P (1997) Photosynthetic rate derived from satellite based chlorophyll concentration. *Limnol Oceanogr* 42:1–20. doi:10.4319/lo.1997.42.1.0001
- Bosilovich M, Robertson F, Chen J (2011) Global energy and water budgets in MERRA. *J Clim* 24:5721–5739. doi:10.1175/2011JCLI4175.1
- Bourras D (2006) Comparison of five satellite-derived latent heat flux products to moored buoy data. *J Clim* 19:6292–6313. doi:10.1175/JCLI3977.1
- Brunke M, Wang Z, Zeng X, Bosilovich M, Shie C-L (2011) An assessment of the uncertainties in ocean surface turbulent fluxes in 11 reanalysis, satellite-derived, and combined global datasets. *J Clim* 24(21):5469–5493. doi:10.1175/2011JCLI4223.1
- Businger J, Wyngaard J, Izumi Y, Bradley E (1971) Flux–profile relationships in the atmospheric surface layer. *J Atmos Sci* 28:181–189. doi:10.1175/1520-0469(1971)028<0181:FPRITA>2.0.CO;2
- Clarizia M, Gommenginger C, Bisceglie M, Galdi C, Srokosz M (2012) Simulation of L-band bistatic returns from the ocean surface: a facet approach with application to ocean GNSS reflectometry. *IEEE Trans Geosci Remote Sens* 50:960–971. doi:10.1109/TGRS.2011.2162245
- Clayson C, Roberts J, Bogdanoff A (2014) Seaflux version 1: a new satellite-based ocean–atmosphere turbulent flux dataset. *Int J Climatol* (submitted)
- Fairall C, Bradley E, Godfrey J, Wick G, Edson J, Young G (1996) Cool-skin and warm-layer effects on sea surface temperature. *J Geophys Res* 101(C1):1295–1308. doi:10.1029/95JC03190
- Falkowski P, Raven J (2007) Aquatic photosynthesis, 2nd edn. Princeton University Press, Princeton
- Farouki O (1982) Thermal properties of soils. CRREL Monogr No. 81-1. U.S. Army Cold Regions Research and Engineering Laboratory
- Fu Q, Liou K (1993) Parameterization of the radiative properties of cirrus clouds. *J Atmos Sci* 50:2008–2025. doi:10.1175/1520-0469(1993)050<2008:POTRPO>2.0.CO;2
- Gilichinsky D, Barry R, Bykhovets S, Sorokovikov V, Zhang T, Zudin S, Fedorov-Davydov D (1998) A century of temperature observations of soil climate: methods of analysis and long-term trends. In: Lewkowicz A, Allard M (eds) Proceedings of the 7th international conference on permafrost, June 23–27, 1998, Yellowknife, Canada, Nordicana, vol 57. University of Laval, Quebec, pp 313–317
- Heitman J, Xiao X, Horton R, Sauer T (2008) Sensible heat measurements indicating depth and magnitude of subsurface soil water evaporation. *Water Resour Res* 44(4):W00D05. doi:10.1029/2008WR006961
- Heitman J, Horton R, Sauer T, Ren T, Xiao X (2010) Latent heat in soil heat flux measurements. *Agric For Meteorol* 150(7–8):1147–1153. doi:10.1016/j.agrformet.2010.04.017
- Huang S, Deng Y, Wang J (2014) Re-evaluation of the Earth’s surface energy balance using a new method of heat fluxes. American Geophysical Union Fall Meeting, San Francisco, A41B-3022
- Jiménez C, Prigent C, Mueller B, Seneviratne S, McCabe M, Wood E, Rossow W, Balsamo G, Betts A, Dirmeyer P, Fisher J, Jung M, Kanamitsu M, Reichle R, Reichstein M, Rodell M, Sheffield J, Tu K, Wang K (2011) Global intercomparison of 12 land surface heat flux estimates. *J Geophys Res Atmos* 116:D02102. doi:10.1029/2010JD014545
- Jung M, Reichstein M, Ciais P, Seneviratne S, Sheffield J, Goulden M, Bonan G, Cescatti A, Chen J, de Jeu R, Dolman A, Eugster W, Gerten D, Gianelle D, Gobron N, Heinke J, Kimball J, Law B, Montagnani L, Mu Q, Mueller B, Oleson K, Papale D, Richardson A, Rouspard O, Running S, Tomelleri E, Viovy N, Weber U, Williams C, Wood E, Zaehle S, Zhang K (2010) Recent decline in the global land evapotranspiration trend due to limited moisture supply. *Nature* 467:951–954. doi:10.1038/nature09396
- Kato S, Loeb N, Rutan D, Rose F, Sun-Mack S, Miller W, Chen Y (2012) Uncertainty estimate of surface irradiances computed with MODIS-, CALIPSO-, and CloudSat-Derived cloud and aerosol properties. *Surv Geophys* 33:395–412. doi:10.1007/s10712-012-9179-x
- Katzberg S, Dunion J (2009) Comparison of reflected GPS wind speed retrievals with dropsondes in tropical cyclones. *Geophys Res Lett* 36:L17602. doi:10.1029/2009GL039512
- Katzberg S, Walker R, Roles J, Lynch T, Black P (2001) First GPS signals reflected from the interior of a tropical storm: preliminary results from Hurricane Michael. *Geophys Res Lett* 28:1981–1984. doi:10.1029/2000GL012823
- Komjathy A, Armatys M, Masters D, Axelrad P, Zavorotny V, Katzberg S (2004) Retrieval of ocean surface wind speed and wind direction using reflected GPS signals. *J Atmos Ocean Technol* 21:515–526. doi:10.1175/1520-0426(2004)021<0515:ROOSWS>2.0.CO;2
- Koster R, Suarez M, Ducharne A, Stieglitz M, Kumar P (2000) A catchment-based approach to modeling land surface processes in

- a general circulation model: 1—model structure. *J Geophys Res* 105(D20):24809–24822. doi:[10.1029/2000JD900327](https://doi.org/10.1029/2000JD900327)
- Kuhlbrodt T, Gregory J (2012) Ocean heat uptake and its consequences for the magnitude of sea level rise and climate change. *Geophys Res Lett* 39:L18608. doi:[10.1029/2012GL052952](https://doi.org/10.1029/2012GL052952)
- Lakshmi V (2013) Remote sensing of soil moisture review article. *ISRN Soil Sci* 2013, Article ID 424178, p 33 doi:[10.1007/s11707-009-0023-7](https://doi.org/10.1007/s11707-009-0023-7)
- Laurent L, Simmons H (2006) Estimates of power consumed by mixing in the ocean interior. *J Clim* 19:4877–4890. doi:[10.1175/JCLI3887.1](https://doi.org/10.1175/JCLI3887.1)
- Levitus S, Antonov J, Boyer T, Baranova O, Garcia H, Locarnini R, Mishonov A, Reagan J, Seidov D, Yarosh E, Zweng M (2012) World ocean heat content and thermohaline sea level change (0–2000 m), 1955–2010. *Geophys Res Lett* 39:L10603. doi:[10.1029/2012GL051106](https://doi.org/10.1029/2012GL051106)
- Liu H, Lin W, Zhang M (2010) Heat budget of the upper ocean in the south-central equatorial Pacific. *J Clim* 23:1779–1792. doi:[10.1175/2009JCLI3135.1](https://doi.org/10.1175/2009JCLI3135.1)
- Moore G, Renfrew I (2002) An assessment of the surface turbulent heat fluxes from the NCEP–NCAR reanalysis over the western boundary currents. *J Clim* 15:2020–2037. doi:[10.1175/1520-0442\(2002\)015<2020:AAOTST>2.0.CO;2](https://doi.org/10.1175/1520-0442(2002)015<2020:AAOTST>2.0.CO;2)
- Mueller B, Seneviratne S, Jiménez C, Corti T, Hirschi M, Balsamo G, Ciaia P, Dirmeyer P, Fisher J, Guo Z, Jung M, Maignan F, McCabe M, Reichle R, Reichstein M, Rodell M, Sheffield J, Teuling A, Wang K, Wood E, Zhang Y (2011) Evaluation of global observations-based evapotranspiration datasets and IPCC AR4 simulations. *Geophys Res Lett* 38:L06402. doi:[10.1029/2010GL046230](https://doi.org/10.1029/2010GL046230)
- Mueller B, Hirschi M, Jiménez C, Ciaia P, Dirmeyer P, Dolman A, Fisher J, Jung M, Ludwig F, Maignan F, Miralles D, McCabe M, Reichstein M, Sheffield J, Wang K, Wood E, Zhang Y, Seneviratne S (2013) Benchmark products for land evapotranspiration: landFlux-EVAL multi-data set synthesis. *Hydrol Earth Syst Sci* 17:3707–3720. doi:[10.5194/hess-17-3707-2013](https://doi.org/10.5194/hess-17-3707-2013)
- Nachtergaele F, Velthuizen H, Verelst L, Wiberg D et al (2012) Harmonized world soil database (version 1.2). FAO, Rome
- Nearing S, Moran M, Scott R, Ponce-Campos G (2012) Coupling diffusion and maximum entropy models to estimate thermal inertia. *Remote Sens Environ* 119:222–231. doi:[10.1016/j.rse.2011.12.012](https://doi.org/10.1016/j.rse.2011.12.012)
- Ochsner T, Sauer T, Horton R (2006) Field tests of the soil heat flux plate method and some alternatives. *Agron J* 98:1005–1014. doi:[10.2134/agronj2005.0249](https://doi.org/10.2134/agronj2005.0249)
- Owe M, De Jeu R, Holmes T (2008) Multisensor historical climatology of satellite-derived global land surface moisture. *J Geophys Res* 113:F01002. doi:[10.1029/2007JF000769](https://doi.org/10.1029/2007JF000769)
- Pan H, Mahrt L (1987) Interaction between soil hydrology and boundary layer developments. *Bound-Layer Meteorol* 38:185–202. doi:[10.1007/BF00121563](https://doi.org/10.1007/BF00121563)
- Pisciotta J, Zou Y, Baskakov I (2010) Light-dependent electrogenic activity of Cyanobacteria. *PLoS One* 5:e10821. doi:[10.1371/journal.pone.0010821](https://doi.org/10.1371/journal.pone.0010821)
- Qian B, Gregorich E, Gameda S, Hopkins D, Wang X (2011) Observed soil temperature trends associated with climate change in Canada. *J Geophys Res Atmos* 116:D02106. doi:[10.1029/2010JD015012](https://doi.org/10.1029/2010JD015012)
- Renfrew I, Moore G, Guest P, Bumke K (2002) A comparison of surface layer and surface turbulent flux observations over the Labrador Sea with ECMWF analyses and NCEP reanalyses. *J Phys Oceanogr* 32:383–400. doi:[10.1175/1520-0485\(2002\)032<0383:ACOSLA>2.0.CO;2](https://doi.org/10.1175/1520-0485(2002)032<0383:ACOSLA>2.0.CO;2)
- Rienecker M, Suarez M, Gelaro R et al (2011) MERRA: NASA's modern-era retrospective analysis for research and applications. *J Clim* 24:3624–3648. doi:[10.1175/JCLI-D-11-00015.1](https://doi.org/10.1175/JCLI-D-11-00015.1)
- Roberts J, Robertson F, Clayson C, Bosilovich M (2012) Characterization of turbulent latent and sensible heat flux exchange between the atmosphere and ocean in MERRA. *J Clim* 25(3):821–838. doi:[10.1175/JCLI-D-11-00029.1](https://doi.org/10.1175/JCLI-D-11-00029.1)
- Rodell M, Houser P, Jambor U, Gottschalck J, Mitchell K, Meng C, Arsenault K, Cosgrove B, Radakovich J, Bosilovich M, Entin J, Walker J, Lohmann D, Toll D (2004) The global land data assimilation system. *Bull Am Meteorol Soc* 85:381–394. doi:[10.1175/BAMS-85-3-381](https://doi.org/10.1175/BAMS-85-3-381)
- Saunders P (1967) Temperature at the ocean–air interface. *J Atmos Sci* 24:269–273. doi:[10.1175/1520-0469\(1967\)024<0269:TTATOA>2.0.CO;2](https://doi.org/10.1175/1520-0469(1967)024<0269:TTATOA>2.0.CO;2)
- Shanafield M, Cook P, Gutiérrez-Jurado H, Faux R, Cleverly J, Eamus D (2015) Field comparison of methods for estimating groundwater discharge by evaporation and evapotranspiration in an arid-zone playa. *J Hydrol* 527:1073–1083. doi:[10.1016/j.jhydrol.2015.06.003](https://doi.org/10.1016/j.jhydrol.2015.06.003)
- Stephens G, Li J, Wild M, Clayson C, Loeb N, Kato S, L'Ecuyer T, Stackhouse P Jr, Lebsock M, Andrews T (2012) An update on Earth's energy balance in light of the latest global observations. *Nature Geosci* 5:691–696. doi:[10.1038/ngeo1580](https://doi.org/10.1038/ngeo1580)
- Stull R (1988) An introduction to boundary layer meteorology. Kluwer Academic Publishers, New York
- Toggweiler J, Samuels B (1998) On the ocean's large-scale circulation near the limit of no vertical mixing. *J Phys Oceanogr* 28:1832–1852. doi:[10.1175/1520-0485\(1998\)028<1832:OTOSLS>2.0.CO;2](https://doi.org/10.1175/1520-0485(1998)028<1832:OTOSLS>2.0.CO;2)
- Townshend J (1992) Improved global data for land applications. IGBP global change report no. 20, International Geosphere–Biosphere Programme, Stockholm
- Trenberth K, Fasullo J, Kiehl J (2009) Earth's global energy budget. *Bull Am Meteorol Soc* 90:311–323. doi:[10.1175/2008BAMS2634.1](https://doi.org/10.1175/2008BAMS2634.1)
- Vinukollu R, Meynadier R, Sheffield J, Wood E (2011) Multi-model, multi-sensor estimates of global evapotranspiration: climatology, uncertainties and trends. *Hydrol Process* 25:3993–4010. doi:[10.1002/hyp.8393](https://doi.org/10.1002/hyp.8393)
- Wang J, Bras R (2009) A model of surface heat fluxes based on the theory of maximum entropy production. *Water Resour Res* 45:W11422. doi:[10.1029/2009WR007900](https://doi.org/10.1029/2009WR007900)
- Wang J, Bras R (2010) An extremum solution of Monin–Obukhov similarity equations. *J Atmos Sci* 67:485–499. doi:[10.1175/2009JAS3117.1](https://doi.org/10.1175/2009JAS3117.1)
- Wang J, Bras R (2011) A model of evapotranspiration based on the theory of maximum entropy production. *Water Resour Res* 47:W03521. doi:[10.1029/2010WR009392](https://doi.org/10.1029/2010WR009392)
- Wang K, Dickinson R (2012) A review of global terrestrial evapotranspiration: observation, modeling, climatology, and climatic variability. *Rev Geophys* 50:RG2005. doi:[10.1029/2011RG000373](https://doi.org/10.1029/2011RG000373)
- Wang J, Bras R, Sivandran G, Knox R (2010) A simple method for the estimation of thermal inertia. *Geophys Res Lett* 37:L05404. doi:[10.1029/2009GL041851](https://doi.org/10.1029/2009GL041851)
- Wang W, Xie P, Yoo S, Xue Y, Kumar A, Wu X (2011) An assessment of the surface climate in the NCEP climate forecast system reanalysis. *Clim Dyn* 37:1601–1620. doi:[10.1007/s00382-010-0935-7](https://doi.org/10.1007/s00382-010-0935-7)
- Wang J, Bras R, Nieves V, Deng Y (2014) A model of energy budget over water, snow and ice surfaces. *J Geophys Res Atmos* 119:6034–6051. doi:[10.1002/2013JD021150](https://doi.org/10.1002/2013JD021150)
- Weller G (1968) Heat-energy transfer through a four-layer system: air, snow, sea ice, sea water. *J Geophys Res* 73(4):1209–1220. doi:[10.1029/JB073i004p01209](https://doi.org/10.1029/JB073i004p01209)
- Wielicki B, Barkstrom B, Harrison E, Lee R, Smith G, Cooper J (1996) Clouds and the Earth's radiant energy system (CERES): an Earth observing system experiment. *Bull Am Meteorol Soc* 77:853–868. doi:[10.1175/1520-0477\(1996\)077<0853:CATERE>2.0.CO;2](https://doi.org/10.1175/1520-0477(1996)077<0853:CATERE>2.0.CO;2)

- Yang J, Wang Z (2014) Land surface energy partitioning revisited: a novel approach based on single depth soil measurement. *Geophys Res Lett* 41:8348–8358. doi:[10.1002/2014GL062041](https://doi.org/10.1002/2014GL062041)
- Yi Y, Kimball J, Jones L, Reichle R, McDonald K (2011) Evaluation of MERRA land surface estimates in preparation for the soil moisture active passive mission. *J Clim* 24:3797–3816. doi:[10.1175/2011JCLI4034.1](https://doi.org/10.1175/2011JCLI4034.1)
- Yu L, Weller R (2012) 50 year global ocean surface heat flux analysis. FY2012 Annual report, Woods Hole Oceanographic Institution, p 13
- Yu L, Jin X, Weller R (2008) Multidecade global flux datasets from the objectively analyzed air–sea fluxes (OAFlux) Project: latent and sensible heat fluxes, ocean evaporation, and related surface meteorological variables. Woods Hole Oceanographic Institution, OAFlux project technical report. OA-2008-01, Woods Hole. Massachusetts, p 64
- Yuan W, Liu S, Yu G, Bonnefond J, Chen J, Davis K, Desai A, Goldstein A, Gianelle D, Rossi F, Suyker A, Verma S (2010) Global estimates of evapotranspiration and gross primary production based on MODIS and global meteorology data. *Remote Sens Environ* 114:1416–1431. doi:[10.1016/j.rse.2010.01.022](https://doi.org/10.1016/j.rse.2010.01.022)
- Zeng X, Zhao M, Dickinson R (1998) Intercomparison of bulk aerodynamic algorithms for the computation of sea surface fluxes using TOGA COARE and TAO data. *J Clim* 11:2628–2644. doi:[10.1175/1520-0442\(1998\)011<2628:IOBAAF>2.0.CO;2](https://doi.org/10.1175/1520-0442(1998)011<2628:IOBAAF>2.0.CO;2)
- Zhang K, Kimball J, Nemani R, Running S (2010) A continuous satellite-derived global record of land surface evapotranspiration from 1983 to 2006. *Water Resour Res* 46:W09522. doi:[10.1029/2009WR008800](https://doi.org/10.1029/2009WR008800)